Loading rate dependence of permeability evolution in porous aeolian sandstones

Loading rate dependence of permeability evolution in porous aeolian sandstones

Ira O. Ojala, Bryne T. Ngwenya, and Ian G. Main
School of GeoSciences, University of Edinburgh, Edinburgh, UK

Received 13 December 2002; revised 19 September 2003; accepted 8 October 2003; published 17 January 2004.

[1] Mechanical properties of rocks are characterized by their notable dependence on the applied deformation rate. However, little is known about the strain rate dependence of fluid flow properties since most laboratory tests are conducted using a single, high strain rate. We have investigated the effect of loading rate on the permeability of porous sandstones by carrying out triaxial compression tests at four different temperatures and strain rates with continuous monitoring of permeability, acoustic emission (AE), and pore fluid chemistry. All tests are characterized by an initial permeability decrease due to inferred compaction of favorably oriented cracks. The amount of initial permeability reduction increases with decreasing strain rate, thus implying a more efficient initial compaction at slower strain rates. At a later stage of loading, permeability correlates with stress, ion concentration, or AE damage depending on the strain rate used. High strain rate tests are characterized by a positive power law or logarithmic correlation between permeability and AE damage. At slow strain rates, permeabilities decrease exponentially with mean effective stress and axial strain for the Locharbriggs sandstone. The Clashach sandstone exhibits a linear correlation between permeability and exit pore fluid concentrations (Si, Mg, Fe, Al) if a slow strain rate is used. These observations have important implications for the applicability of room temperature, high strain rate laboratory data to the conditions that prevail in the Earth's crust. *INDEX TERMS:* 1045 Geochemistry: Low-temperature geochemistry; 5102 Physical Properties of Rocks: Acoustic properties; 5104 Physical Properties of Rocks: Fracture and flow; 5114 Physical Properties of Rocks: Permeability and porosity; *KEYWORDS:* permeability, deformation rate, acoustic emission

Citation: Ojala, I. O., B. T. Ngwenya, and I. G. Main (2004), Loading rate dependence of permeability evolution in porous aeolian sandstones, *J. Geophys. Res.*, *109*, B01204, doi:10.1029/2002JB002347.

1. Introduction

[2] Permeability is one the most important material properties of the rocks that make up the Earth's crust. It is of economic and scientific interest of its own right, but also because of the strong coupling of fluid flow with many mechanical, thermal and chemical processes operating in the crust. The behavior of hydrothermal systems, ore and hydrocarbon deposits are all governed by the movement of fluids. Similarly, both mechanical and seismic responses of the crust are strongly influenced by fluid flow. There are several lines of evidence for the existence of fluid-rock interaction at all crustal levels [*Sornette*, 1999]. For instance, fracture surfaces commonly possess visible signs of dissolution and recrystallization. Such mineral alteration may vary from the growth of single crystals to total infilling of fractures [e.g., *Sibson*, 1994]. Fluids have also been directly sampled in superdeep wells thus confirming the presence of water and fluid filled fractures over 9 km depth [*Huenges et al.*, 1997].

[3] Although a key material property, permeability is notoriously difficult to estimate. The permeability of rocks varies over 10 orders of magnitude (10^{-24} to 10^{-12} m^2) [*Brace*, 1980] and hence it may be hard to provide even an order of magnitude estimate. Furthermore, crustal rocks are exposed to a wide range of temperature, pore pressure and deviatoric stress conditions and all of these parameters may induce major changes in fluid flow properties [*Guéguen and Palciauskas*, 1994]. Pore pressure tends to open up fractures thus enhancing fluid flow, while the effect of lithostatic stress is to decrease permeability by progressive pore closure. High temperature or deviatoric stress may induce microfracturing and increase permeability. Fluid flow properties can also be modified by changes in pore microstructure resulting from chemical processes, such as clay swelling and dissolution-precipitation reactions [*Tenthorey et al.*, 1998]. In general, permeability increases where material is being dissolved and it decreases due to clogging of pore necks by mineral precipitation. The kinetic processes that drive dissolution-precipitation reactions are controlled by various parameters, such as temperature, stress and fluid composition. However, the relationship between chemical reaction and permeability change is not well understood.

[4] Laboratory experiments under controlled conditions provide a good opportunity to investigate the coupling of fluid flow with brittle fracturing and chemical reaction. The

0148-0227/04/2002JB002347$09.00

results of triaxial compression tests have shown that dilatancy precedes failure by brittle faulting in both low- and high-porosity rocks [*Brace et al.*, 1966; *Scholz*, 1968; *Zoback and Byerlee*, 1975]. The onset of dilatancy is marked C', denoting the stress level at which the relationship between stress and volumetric strain deviates from linearity. Such increase in sample porosity typically begins at half of the peak stress of the specimen [*Scholz*, 1968] and it can be attributed to the growth of axial microcracks in the direction of maximum compressive stress [*Tapponier and Brace*, 1976]. Porosity and permeability are often assumed [*Carman*, 1956; *Seeburger and Nur*, 1984; *Guéguen and Dienes*, 1989; *Bernabé*, 1995; *Zhu et al.*, 1999; *Simpson et al.*, 2001] and more rarely, observed [*Bourbie and Zinszner*, 1985; *Zhang et al.*, 1994; *Popp et al.*, 2001] to be positively correlated. Hence the evolution of permeability is expected to be coupled to the increase in volumetric strain during dilatancy. In fact, such positive correlation has been observed for low-porosity rocks, with permeabilities increasing by a factor of two to eight during the dilatant phase of deformation [*Zoback and Byerlee*, 1975; *Zhang et al.*, 1994; *Kiyama et al.*, 1996]. However, for high-porosity rocks ($\phi > 15\%$) the situation is more problematic.

[5] Previous experimental studies on a variety of sandstones have reported both increasing [*Mordecai and Morris*, 1971] and decreasing permeabilities [*Zhu and Wong*, 1997] during the dilatant phase of microcracking. Furthermore, the same rock type may exhibit both increasing and decreasing permeabilities during dilatancy, as was observed for Darley Dale sandstone by *Zhu and Wong* [1997]. In order to characterize the evolution path for microcrack induced dilatancy and sample permeability, they introduced a parameter ξ that is given by

$$\xi = \frac{k_{\text{peak}}}{k(C')} - 1 \tag{1}$$

where $k(C')$ and k_{peak} are the permeabilities at the onset of dilatancy and peak stress, respectively. The correlation parameter ξ decreases with increasing initial porosity of the test specimen and its sign indicates whether porosity and permeability changes are positively or negatively correlated [*Wong and Zhu*, 1999]. Specimen with porosities of 15% or over are consistently associated with negative ξ values. Hence the contradictory behavior observed for Darley Dale sandstone can be explained by different initial porosities of the test specimen.

[6] The equivalent channel model [*Paterson*, 1983; *Walsh and Brace*, 1984] can be used to provide a qualitative explanation of the observed negative correlation between permeability and porosity changes in high-porosity rocks. It relates permeability k to porosity ϕ by

$$k = C\frac{m^2\,\phi}{\tau} \tag{2}$$

where m is the hydraulic radius, τ is tortuosity, and C is 1/2 and 1/3 for circular tubes and cracks, respectively. Hence permeability may decrease in a dilating rock sample if the hydraulic radius is decreasing with progressively increasing tortuosity of the flow path [*Zhu and Wong*, 1996]. Other workers have argued that tortuosity is merely a "fudge factor" that is used to make theoretical calculations to fit experimental data [*Fatt*, 1956]. The problem with decreasing permeability that is associated with dilatancy stems from the idea that porosity and permeability should be interrelated. However, permeability is essentially a geometric property and it is measured in square meters. Hence there may be no need to invoke a direct correlation between permeability and porosity [*Scheidegger*, 1974; *Guéguen and Palciauskas*, 1994]. Moreover, if rock pore structure is considered to be fractal [*Thompson*, 1991], such an assumption precludes the use of an effective length scale that the concept of geometric tortuosity is based on [*Clennell*, 1997].

[7] In other models, permeability is assumed to decrease exponentially with the effective mean stress. The effect of increasing stress is to decrease sample permeability by elastic pore closure. The reduction in permeability is given by

$$k = k_0 \exp[-\gamma\,(\sigma_{\text{eff}} - \sigma_0)] \tag{3}$$

where σ_{eff} is the effective mean stress, σ_0 is its starting value, and γ is a stress sensitivity coefficient [*Rice*, 1992]. Recently, *Wong and Zhu* [1999] presented a compilation of the measured γ values for different geomaterials. While porous rocks were characterized by $\gamma < 0.02$ MPa^{-1}, fractured rocks and tight sandstones exhibited higher values of the stress sensitivity coefficient γ. However, other workers have suggested that permeability should be related to axial strain, rather than stress since it is a geometric property [*David et al.*, 1994; *Main et al.*, 2000]. In their models, axial strain replaces $\sigma_{\text{eff}} - \sigma_0$ in equation (3).

[8] Exponentially decreasing permeabilities have also been observed in the absence of significant porosity loss due to elastic compaction. Experimental work relating permeability to chemical reactions have demonstrated that permeability reduction of several orders of magnitude can be attributed to the precipitation of authigenic phases [*Morrow et al.*, 1981; *Moore et al.*, 1983; *Small et al.*, 1992; *Ngwenya et al.*, 1995; *Scholz et al.*, 1995; *Tenthorey et al.*, 1998; *Morrow et al.*, 2001]. Such experiments are typically carried out under constant effective pressure. If pressure solution is investigated, a small end load may also be applied. Both power law [*Aharonov et al.*, 1998] and exponential [*Morrow et al.*, 2001] decreases in permeability have been observed in such studies. The reduction in permeability can be explained by increasing roughness of the pore geometry that is caused by mineral precipitation [*Aharonov et al.*, 1998].

[9] In this study we have addressed the coupling of fluid flow with brittle fracturing and chemical reaction in two high-porosity ($\phi = 10$–17%) aeolian sandstones. While previous studies have invariably monitored these effects separately, in our triaxial compression tests the axial permeability, pore fluid chemistry, and acoustic emission (AE) activity were measured continuously and contemporaneously. In particular, we were aiming to quantify the effect of loading rate and temperature on the permeability evolution during nonhydrostatic loading. Hence the deformation tests were carried out at strain rates of 10^{-5} to 10^{-8} s^{-1} and at temperatures ranging from 25 to 80°C. The AE technique [*Lockner*, 1993] was used as a remote way of monitoring

microcrack damage, since previous work of *Scholz* [1968] and *Sano et al.* [1981] has shown a direct proportionality between cumulative AE event rate and inelastic volumetric strain. The results of our experiments demonstrate that both Clashach and Locharbriggs sandstone display a distinct loading rate dependence of axial permeability. At high strain rates of 10^{-5} and 10^{-6} s^{-1}, permeability correlates with microcrack damage derived from the AE catalogue, thus indicating a positive correlation between porosity and permeability. In contrast, the use of a low strain rate results in permeability evolution that is controlled by differential stress and pore fluid chemistry for the Locharbriggs and Clashach specimens, respectively. The strong correlation between the chemical dissolution and microcrack damage for the Locharbriggs slow strain rate tests here has been previously reported by *Ojala et al.* [2003]. However, in this study we concentrate solely on the permeability evolution and its correlation with loading rate, effective mean stress, axial strain, AE activity, and pore fluid chemistry.

2. Methodology

[10] The experiments were carried out on two Permian aeolian sandstones. One block of the Hopeman sandstone was obtained from the Clashach quarry in northeast Scotland, and another block was obtained from the Locharbriggs quarry in southwest Scotland. A mineralogical characterization of these sandstones has been provided by *Crawford et al.* [1995]. The Clashach sandstone is well-sorted, medium- to coarse-grained (250–500 μm) subarcosic arenite that is composed of 89% quartz and 11% feldspar. The Clashach samples are characterized by pervasive cementation due to quartz overgrowths. Locharbriggs sandstone has a smaller grain size of 100 μm, and it is composed of 83% quartz, 16% feldspar, and 1% hematite. The Locharbriggs sandstone is relatively weakly cemented with a diagenetic assemblage that is characterized by hematite and illite coatings on grain surfaces.

[11] Cylindrical samples measuring 80 mm in length and 38 mm in diameter were cut from fresh, unweathered sandstone blocks. The Locharbriggs samples were cut parallel to lamination. Because of the lack of discernible fabric the Clashach cores were cut in two orthogonal directions. The total porosities of the samples were measured using the density method [*Guéguen and Palciauskas*, 1994], while the interconnected porosities were determined from the weight difference between wet and dry cores. The interconnected porosities ranged between 10–12% and 15–17% for Clashach and Locharbriggs sandstones, respectively. The total porosities were typically about 6% higher [*Ojala et al.*, 2003].

[12] The test methodology was essentially the same as by *Ojala et al.* [2003]. The samples were deformed in a conventional triaxial ($\sigma_1 > \sigma_2 = \sigma_3$) testing apparatus under constant flow through conditions. The flow of water in and out of the sample equaled 0.2 min min^{-1}, since the outflow rate could be determined independently from the weight of the chemical samples. The confining pressure was fixed within the brittle regime at 13.5 MPa. The ambient back pressure was equal to atmospheric pressure at 0.1 MPa. Initially, the jacketed sample was heated to the appropriate temperature and loaded to hydrostatic conditions. In order to remove highly reactive fine particles the specimen was then flushed with distilled water for 24 hours at constant fluid flow rate of 0.2 mL min^{-1}. Time and temperature dependence of permeability was investigated by carrying out tests at temperatures of 25–80°C using four different loading rates. The strain rates used for the tests ranged from 10^{-5} to 10^{-8} s^{-1} during the linear elastic phase of deformation.

[13] The axial permeability was determined from the pressure difference dP across the test specimen by using a high-sensitivity Validyne DP 360 differential pressure transducer. Since the flow rate Q, sample length l, cross-sectional area A, and viscosity η were known, permeability could be calculated from Darcy's law [*Darcy*, 1856] given by

$$k = \frac{Q\eta l}{A\,dP} \tag{4}$$

The evolution of fluid chemistry was assessed by analyzing the amount of dissolved ions in the exit pore fluid throughout the experiments. The exit pore fluid was directed to an autosampler loaded with test tubes. The samples were acidified by using 1% HCl in order to reduce adsorption of dissolved species onto container walls and to stop mineral precipitation. The pore fluid samples were analyzed after the tests for the concentration of Al, Ca, Fe, K, Mg, Na, and Si by using an inductively coupled plasma source (ICP-AES). The analysis was carried out for these particular ions in order to quantify the extent of chemical dissolution from quartz, feldspar, illite, and diagenetic iron grains in the rock sample. In order to obtain enough sample (5 mL) for analysis of dissolved species, sampling rates of 30 min and 1 hour were used. Hence a clear geochemical signal could only be recorded for the slow strain rate tests at 10^{-7} and 10^{-8} s^{-1}.

[14] The sampling times for the exit pore fluid were corrected for the residence time τ_t, which describes the average time a fluid element resides inside the rock sample. Assuming constant porosity ϕ and constant fluid flow rate Q, the residence time is given by

$$\tau_t = \frac{V_\phi}{Q} \tag{5}$$

where V_ϕ is the pore volume. In analyzing the results, each chemical sample was plotted at a time when it resided halfway inside the rock sample. However, this is only an approximation since τ_t decreases during compactive stage and increases during dilatancy. Assuming 1% variation in rock porosity due to compactive/dilatant processes, the error in τ is 5 min, which represents only 0.5% of the total duration of the 10^{-7} s^{-1} tests.

[15] Although the volumetric strain was not measured, the AE technique was used as a way of remotely monitoring microcrack growth inside the rock sample. The acoustic emission (AE) activity was measured by a Panametrics 125 kHz piezoelectric transducer, and the signals were amplified by 40 dB using a Panametrics preamplifier and recorded using MISTRAS acoustic emission system. To eliminate background noise, the amplitude threshold for the AE signals was set at 50 dB, which is 10 dB higher than the amplitude threshold used in previous tests. The higher-

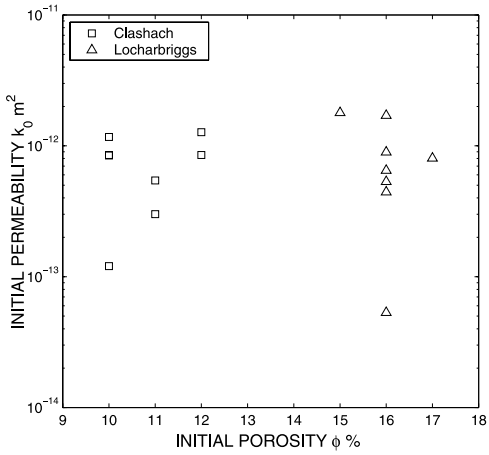

Figure 1. Initial permeability as a function of porosity. For a given porosity value the permeability may range over 2 orders of magnitude. This is likely due to the normal lithological variation in the rock formation.

amplitude threshold was chosen in order to ensure adequate disk space for data storage, especially for the slow strain rate tests that lasted for several days.

[16] Microstructural analysis was carried out in order to compare the deformation styles produced in high and slow strain rate tests and in different test lithologies. Hence thin and polished sections were prepared near midlength of the rock cores in a direction parallel to the shear band. The analysis was carried out by using an optical microscope and a scanning electron microscope at a magnification of 200×. The linear density of cracks was determined from the number of cracks along five traverses totalling 48 mm inside each of four 0.8 × 9.6 mm^2 mosaics of SEM micrographs. The traverse direction and the long direction of the mosaic were aligned parallel to the direction of σ_3. Only transgranular cracks oriented within 45° of the direction of maximum compressive stress were included in the crack count. This is because both grain boundary cracks and transgranular cracks oriented at high angles to σ_1 could have formed or been significantly altered during decompression [*Zhang et al.*, 1994]. Linear crack densities were based on 198 and 289 cracks for the 80°C 10^{-6} and 10^{-8} s^{-1} Locharbriggs samples and 190 and 204 for the Clashach tests.

3. Results

3.1. Initial Permeabilities and the Effect of Loading Rate on Permeability Evolution

[17] The initial permeabilities and porosities for the test specimen are plotted against each other in Figure 1. The initial permeability k_0 was measured under hydrostatic pressure of 13.5 MPa at the start of each test run. The interconnected porosities varied from 10–12% and 15–17% for the Clashach and Locharbriggs sandstone, respectively. The 2% porosity variation resulted in permeabilities spanning over 2 orders of magnitude. For Clashach sandstone the initial permeability ranged from 1.20 to 12.7 × 10^{-13} m^2, while k_0 of Locharbriggs sandstone varied from 0.53 to 17.9 × 10^{-13} m^2. The variability on the recorded permeabilities is due to the normal lithological variation in the sandstone block since permeabilities ranging over 2 orders of magnitude for a given porosity value have also been recorded in previous studies [*Pape et al.*, 1999]. Although the Clashach sample porosities were typically 5% less than the Locharbriggs porosities, the recorded permeabilities were of similar magnitudes. These observations suggests that porosity alone is not sufficient in determining fluid flow properties but some knowledge of the microstructure of porosity is also required.

[18] Triaxial tests were carried out in order to investigate the loading rate and temperature dependence of fluid flow properties in Clashach and Locharbriggs sandstones. Because of the moderate confining pressure (13.5 MPa) used, all the samples failed by shear localization oriented at 26–40° to the direction of maximum compressive stress. There was no correlation of the angle of the fault with temperature or strain rate. Figure 2 illustrates the stress-strain curves for Clashach and Locharbriggs sandstones. For Clashach sandstone a weak strain-hardening phase preceded failure and the associated stress drop. In contrast, the stress-strain behavior of Locharbriggs sandstone was consistently associated with pronounced strain-hardening and -softening phases. It is maybe due to its pervasive quartz cementation that Clashach sandstone was considerably stronger and more brittle than Locharbriggs sandstone (Table 1). While the strength of Locharbriggs sandstone ranged from 78 to 82 MPa, Clashach sandstone was roughly twice as strong with peak stresses in the range of 123 to 169 MPa. Specimen strength and the elastic modulus decreased with decreasing strain rate [*Ojala et al.*, 2003]. The reduced stiffness suggests that a greater amount of microcracking took place in the slow strain rate tests. Test temperature, however, did not affect the stress-strain curves in any systematic manner.

[19] The use of four different strain rates induced significant changes in the evolution of permeability with time. This observation indicates that the dominant mechanism affecting fluid flow properties may change with deformation rate. Figure 3 shows the temporal evolution of permeability for both Locharbriggs and Clashach sandstones. For the Locharbriggs sandstone, high loading rates of 10^{-5} to 10^{-6} s^{-1} caused the permeability to increase in the dilatant phase of microcracking that preceded specimen failure. In contrast, slow loading rates of 10^{-7} and 10^{-8} s^{-1} resulted in continuously decreasing permeabilities. Following sample failure, permeabilities continued to decrease with increasing axial strain. For the 10^{-5} and 10^{-6} s^{-1} tests, no appreciable strain occurred after specimen failure, but permeability kept decreasing. There was a tendency for the initial permeability to decrease with increasing test temperature for the Locharbriggs tests.

[20] The 80°C tests conducted on Clashach sandstone showed a similar pattern of permeability evolution irrespective of the strain rate used (Figure 3a). Initial permeability decrease was followed by increasing permeabilities at a later stage of loading. The permeability decrease can be attributed to inferred compaction of favorably oriented cracks, while the permeability enhancement is caused by inferred dilatancy due to microcracking, as evidenced by the AE activity. *Zhu and Wong* [1997] analyzed the evolution path of permeability for their tests using parameter ξ

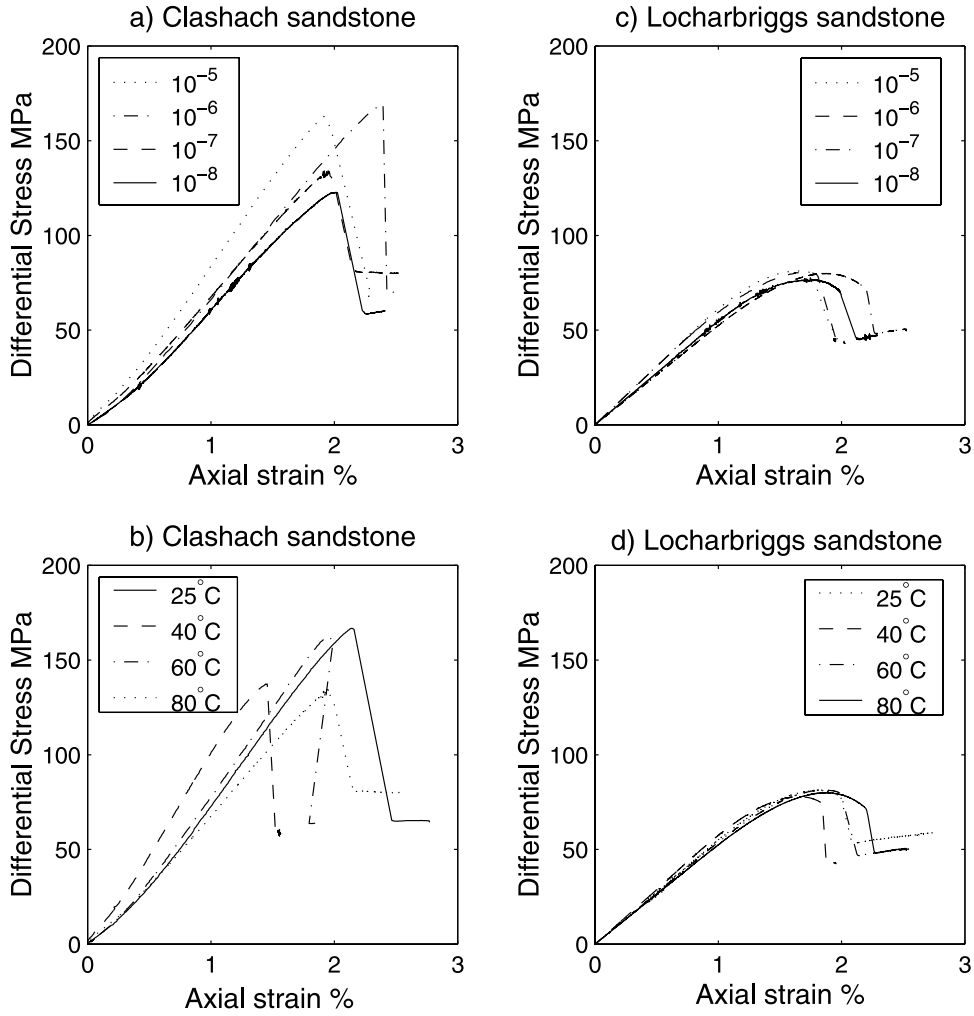

Figure 2. Stress-strain curves for (a) Clashach and (c) Locharbriggs sandstone deformed at a temperature of 80°C with strain rates ranging from 10^{-5} to 10^{-8} s^{-1}. The slow strain rate 10^{-7} s^{-1} tests at T = 25–80°C are also shown for (b) Clashach and (d) Locharbriggs sandstones, respectively. Locharbriggs sandstone showed clear strain-softening and -hardening phases, while Clashach samples were considerably stronger and more brittle with only a weak strain-hardening phase.

Table 1. Mechanical and Permeability Data for the Flow-Through Tests on Clashach and Locharbriggs Sandstones[a]

Rock Type	T, °C	$\dot{\varepsilon}$, s^{-1}	ϕ, %	σ_{max}, MPa	$k_0 \times 10^{-13}$ m^2	k_{peak}, $\times 10^{-13}$ m^2	k_{peak}/k_0, %
Clashach	80	3.1×10^{-5}	10	168.5	11.7	14.3	122
Clashach	80	2.7×10^{-5}	11	162.8	5.44	6.93	127
Clashach	80	3.2×10^{-6}	10	169.3	8.50	7.28	86
Clashach	25	2.5×10^{-7}	10	166.7	8.44	5.47	65
Clashach	40	2.2×10^{-7}	12	140.4	12.7	10.4	82
Clashach	60	2.7×10^{-7}	10	162.8	1.20	0.73	61
Clashach	80	3.3×10^{-7}	12	134.5	8.52	4.16	49
Clashach	80	3.3×10^{-8}	11	122.6	3.01	0.75	25
Locharbriggs	80	3.0×10^{-5}	16	81.2	4.43	4.28	97
Locharbriggs	80	3.2×10^{-6}	16	80.8	5.33	6.70	126
Locharbriggs	25	3.3×10^{-7}	15	81.3	17.9	11.9	67
Locharbriggs	40	2.8×10^{-7}	16	77.8	6.49	3.13	48
Locharbriggs	40	3.3×10^{-7}	16	82.3	17.1	8.56	50
Locharbriggs	60	3.1×10^{-7}	17	81.4	8.04	5.72	66
Locharbriggs	80	3.4×10^{-7}	16	79.9	0.53	0.22	40
Locharbriggs	80	2.8×10^{-8}	16	77.7	8.96	2.98	33

[a]The ϕ is the interconnected porosity.

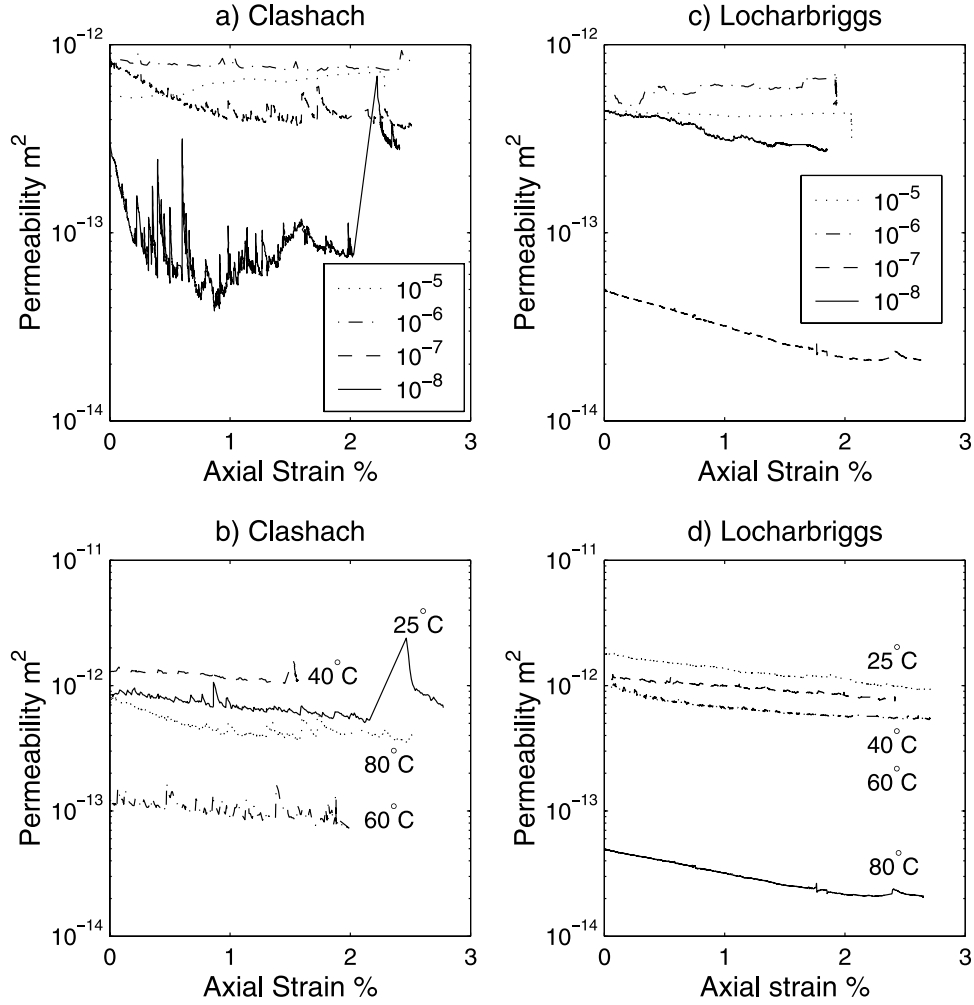

Figure 3. Evolution of permeability with axial strain for (a) Clashach and (c) Locharbriggs sandstone 80°C tests conducted at different strain rates and (b) Clashach and (d) Locharbriggs sandstone deformed at $T = 25–80$°C using a strain rate of 10^{-7} s^{-1}.

(equation (1)), which relates the permeability at the onset of dilatancy to the peak stress permeability. However, the inelastic volumetric strain was not measured for our tests and hence the onset of dilatancy could not be determined uniquely. Instead, we defined parameter k_{min}, which corresponds to the lowest recorded permeability value prior to shear localization. The ratio k_{min}/k_0 was used to assess the relative effect of inferred compaction. Figure 4 illustrates the strain rate effect on k_{min}/k_0, which is given by

$$k_{min}/k_0 = 28.2 \log \dot{\varepsilon} + 228 \quad (6)$$

where $\dot{\varepsilon}$ is the strain rate (in s^{-1}) and k_{min}/k_0 is a percentage. The amount of initial compaction as evidenced by the permeability data was found to be directly proportional to the logarithm of the strain rate used for the tests with an r^2 value of 0.962. At slower strain rates, there was more time available for chemical and mechanical processes to operate, which may have caused more efficient initial compaction of the test specimen and hence a greater decrease in permeability in the early stage of loading. Similarly, the k_{peak}/k_0 ratio was also proportional to the logarithm of strain rate, and it was given by

$$k_{peak}/k_0 = 34.7 \log \dot{\varepsilon} + 280 \quad (7)$$

where the r^2 value was 0.987. At a strain rate of 10^{-5} s^{-1} the peak stress permeability was 22–27% higher than the initial permeability. In contrast, slow strain rate loading at 10^{-8} s^{-1} resulted in significant permeability reduction of 75%. Locharbriggs sandstone also displayed a clear trend of decreasing k_{peak}/k_0 values with deformation rate, as shown in Table 1. Both equations (6) and (7) share a slope that is of similar magnitude, hence suggesting that the strain rate dependence of these two parameters was caused by the same underlying mechanism. However, the k_{peak}/k_{min}, indicating inferred dilatancy, ranged from 101 to 192% and did not display a strain rate dependence (Figure 4c).

[21] The transient increase in permeability at dynamic failure was more frequent for the Clashach tests than for the Locharbriggs tests. Only the 10^{-7} s^{-1} Locharbriggs test showed a transient increase in k at the time intervals used here. In contrast, all of the Clashach tests were characterized

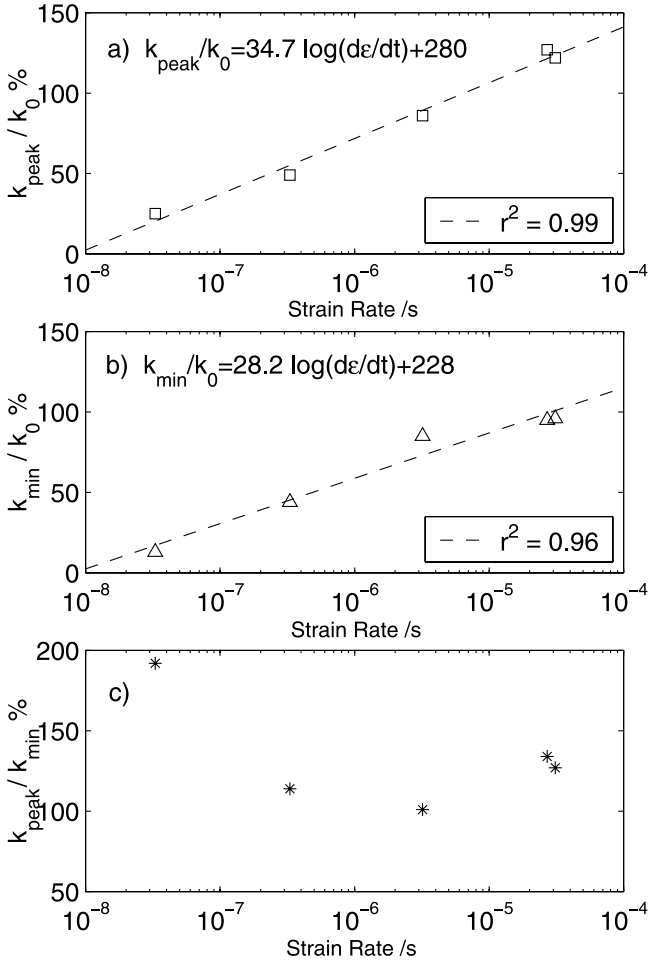

Figure 4. Evolution of permeability dependent on the applied strain rate for the 80°C Clashach tests. (a) Ratio of permeability at peak stress k_{max} to initial permeability k_0 at the start of the test. (b) Ratio of permeability minimum k_{min} to initial permeability k_0 at the start of the test. (c) Ratio of k_{peak} to k_0, which did not display a systematic strain rate dependence.

by a transient k increase associated with the formation of a throughgoing fault. Such transient permeability increase is predicted by the dilatant suction pump model of *Rudnicki and Chen* [1988] that was recently solved by *Grueschow et al.* [2003] for aeolian sandstones similar to those used here. We therefore assume that the dynamic peak in permeability is only apparent. The apparent k increase at failure ranged from 0.2 to 18.6 $\times$ 10^{-13} m^2. The relative change in permeability may, however, be a more appropriate measure of permeability since the absolute value of k was different for each test. The amount of permeability increase varied from 108% for the 10^{-7} s^{-1} test to 887% for the 10^{-8} s^{-1} test. However, there appeared to be no systematic variation between the magnitude of the k increase with the amount of slip δ, the change in shear stress $\Delta\tau$, or the coefficient of friction μ (Table 2). If we assume that the apparent permeability increase is due to the suction pump effect [*Grueschow et al.*, 2003], one would expect a correlation between δ and $\Delta\tau$. However, some of the Clashach data suffered from transient noise peaks due to electrical spikes or disturbances in the fluid flow through the sample. Both of these effects could contribute toward the apparent increase in k that we observe. More detailed modeling would be required to examine this question further.

Table 2. Fault Angle, Friction Coefficient μ, Fault Slip δ, Shear Stress Drop $\Delta\tau$, Apparent Permeability Increase Δk, and Change in Differential Pressure Δp at Dynamic Failure for the Clashach Tests

$\dot{\varepsilon}$, s^{-1}	T, °C	Fault Angle, deg	μ	δ, mm	$\Delta\tau$, MPa	Δk, %	Δp, MPa
3.2 $\times$ 10^{-6}	80	33	0.45	0.02	83.5	28	0.0087
2.5 $\times$ 10^{-7}	25	26	0.78	0.24	90.8	352	0.11
2.2 $\times$ 10^{-7}	40	30	0.58	0.05	65.6	53	0.018
2.7 $\times$ 10^{-7}	60	25	0.84	0.16	86.7	40	0.15
3.3 $\times$ 10^{-7}	80	39	0.21	0.14	31.7	8	0.005
3.3 $\times$ 10^{-8}	80	26	0.78	0.18	54.4	787	0.34

3.2. Microstructural Observations

[22] Intergranular and intragranular fracturing was pervasive in the deformed specimen, suggesting that microfracturing is the cause of the recorded AE activity. Among the mineral components, quartz contained a greater proportion of cracks. Grain boundary opening was also evident in all deformed samples. Oversized pores that contained remnants of feldspar grains were observed in both sandstones, and the origin of these features was attributed to dissolution of feldspar grains. The Clashach fault gouge consisted of partially or wholly fractured grains, indicating cataclasis. Microcracks were preferentially oriented in the direction of the shear band and maximum compressive stress in the 10^{-6} s^{-1} and 10^{-8} s^{-1} strain rate Clashach tests, respectively. The Locharbriggs shear band contained undeformed grains, hence suggesting grain translation and compaction. In addition, Locharbriggs samples did not display a preferential microcrack orientation, possibly because of extensive grain translation. The difference in deformation styles of the high and slow strain rate tests was further investigated by counting the microcrack density of the 80°C Clashach and Locharbriggs tests. The linear crack densities (ρ_c) were higher at the samples that were deformed at a slower strain rate in comparison to the high strain rate samples, as shown in Table 3. The higher crack densities of the slow strain rate tests could be caused by subcritical crack growth, which is likely to be the dominant mechanism for crack propagation in the slow strain rate tests.

3.3. Relationship Between Permeability, Stress, and Strain

[23] The low strain rate tests at 10^{-7} and 10^{-8} s^{-1} on Locharbriggs sandstone exhibited a strong dependence of permeability on stress and strain. Similar pattern of permeability evolution was also observed for the 25 to 60°C tests

Table 3. Linear Crack Densities (ρ_c) in the High and Slow Strain Rate Tests for Both Rock Types

Rock Type	$\dot{\varepsilon}$, s^{-1}	T, °C	Crack ρ_c, mm^{-1}
Clashach	3.2 $\times$ 10^{-6}	80	4.0
Clashach	3.3 $\times$ 10^{-8}	80	4.3
Locharbriggs	3.2 $\times$ 10^{-6}	80	4.1
Locharbriggs	2.8 $\times$ 10^{-8}	80	6.0

Table 4. For the Slow Strain Rate Tests, Permeability k Expressed in Terms of Increasing Stress and Strain According to Equation (3)[a]

Rock	$\dot{\varepsilon}$, s^{-1}	T, °C	γ_1, 10^{-2} MPa^{-1}	r^2	γ_2	r^2
Clashach	2.5×10^{-7}	25	0.81	0.862	22.3	0.860
Clashach	2.2×10^{-7}	40	0.45	0.890	16.3	0.892
Clashach	2.7×10^{-7}	60	0.68	0.544	19.3	0.545
Locharbriggs	3.3×10^{-7}	25	1.56	0.988	25.4	0.984
Locharbriggs	2.8×10^{-7}	40	2.02	0.918	34.1	0.937
Locharbriggs	3.3×10^{-7}	40	0.99	0.953	16.1	0.967
Locharbriggs	3.1×10^{-7}	60	1.64	0.933	25.1	0.920
Locharbriggs	3.4×10^{-7}	80	2.77	0.995	42.0	0.997
Locharbriggs	2.8×10^{-8}	80	2.93	0.985	41.9	0.986

[a]Least squares regression on plots of log k versus mean effective stress or axial strain yielded the stress sensitivity coefficient γ_1 and the strain sensitivity coefficient γ_2, respectively. The goodness of fit is indicated by the r^2 value.

at 10^{-7} s^{-1} conducted on Clashach sandstone. The observation of continuously decreasing permeabilities was best described by an exponential dependence on effective mean stress or axial strain [*Rice*, 1992; *Main et al.*, 2000; *Wong and Zhu*, 1999]. The stress and strain sensitivity parameters γ_1 and γ_2 for the slow loading tests that exhibited decreasing permeabilities were obtained by least squares regression on log linear plots of permeability versus effective mean stress or axial strain for the intact rock specimen (Table 4). The similar r^2 values for γ_1 and γ_2 suggest that the exponential fit to both stress and strain data is equally good. The values of the stress sensitivity parameter γ_1 were consistently smaller for the Clashach tests ($0.5–0.8 \times 10^{-2}$ MPa^{-1}) than for the Locharbriggs sandstone ($1.0–2.8 \times 10^{-2}$ MPa^{-1}). Similarly, the strain sensitivity of permeability evolution as expressed by γ_2 was also smaller for the Clashach tests. While the permeability evolution of the slow strain rate tests on Locharbriggs sandstone was clearly controlled by stress and strain, the lower temperature Clashach tests showed only a moderate dependence of permeability on the applied load.

3.4. Relationship Between Permeability and AE Data

[24] The high strain rate tests at 10^{-5} and 10^{-6} s^{-1} were characterized by a positive correlation between permeability and AE activity. Similar behavior was observed for both sandstones. The occurrence of AE can be related to microfracturing events [*Lockner*, 1993], which may have caused the observed permeability increase by enhancing pore connectivity [*Tapponier and Brace*, 1976]. Hence the cumulative event count N was used to quantify the accumulation of microcrack damage. Figure 5 shows the evolution of permeability and N for Clashach (Figure 5b) and

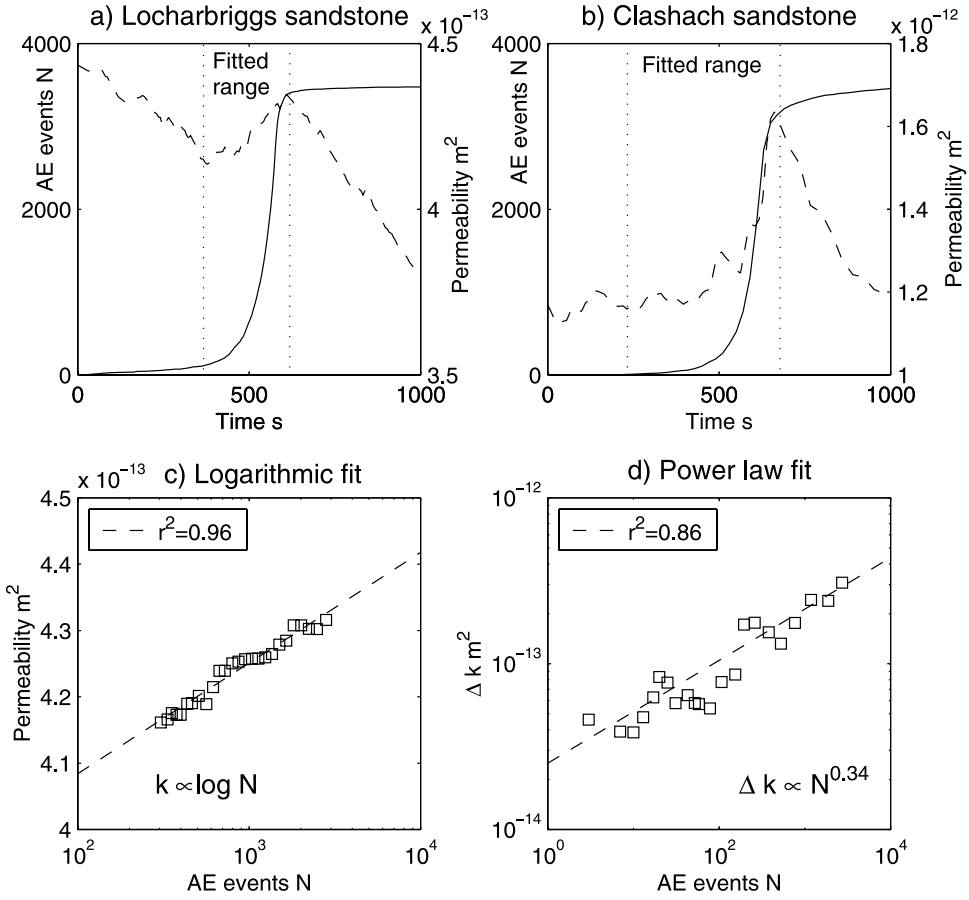

Figure 5. Evolution of permeability and cumulative AE count N as a function of time for two tests conducted at strain rates of (a) 3.1×10^{-5} s^{-1} and (b) 3.0×10^{-5} s^{-1} on Clashach and Locharbriggs sandstones, respectively. The relationship between permeability and cumulative AE count is either (c) a logarithmic or (d) a power law function.

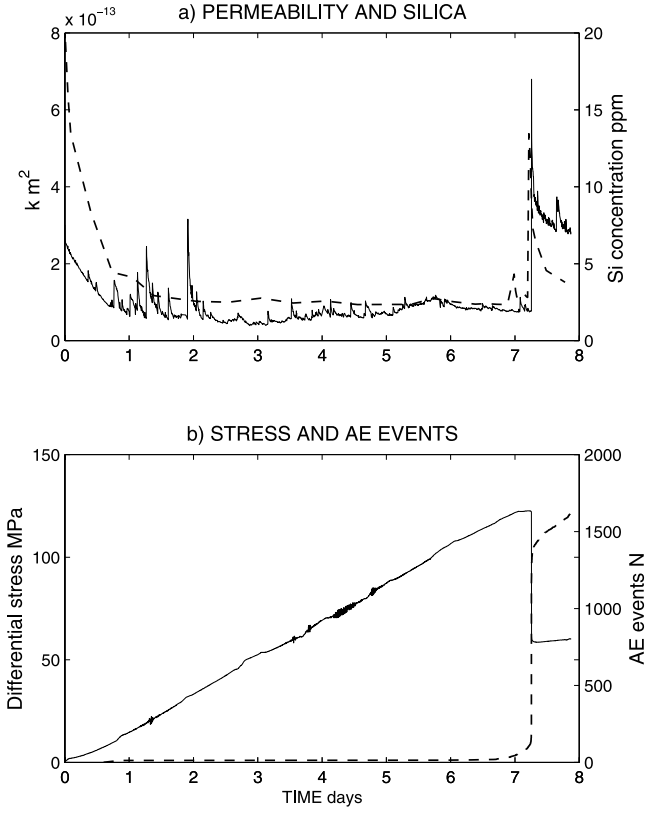

Figure 6. Evolution of (a) permeability and silica concentration (dashed line) and (b) differential stress and cumulative AE event count (dashed line) for a Clashach sandstone 80°C test that was carried out at a strain rate of 3.3×10^{-8} s^{-1}.

Locharbriggs (Figure 5a) sandstone tests conducted at a strain rate of the order of 3×10^{-5} s^{-1}. The initial permeability decrease due to compactive processes was more pronounced for Locharbriggs sandstone. Following the onset of AE activity, the permeabilities started to increase. The permeability maximum was attained just after the formation of a throughgoing fault. The following frictional sliding phase was marked by little or no AE activity. Permeabilities, however, continued to decrease during the postfailure stage. Following specimen failure, permeability no longer correlated with the AE event count.

[25] In the Clashach and Locharbriggs tests conducted at 10^{-5} s^{-1}, sample permeability was directly correlated with the AE activity as shown in Figure 5. For the Clashach test the permeability increase Δk obeyed a power law with respect to N that is given by

$$\Delta k \propto N^{0.34} \tag{8}$$

where the r^2 value is 0.86. The use of a power law was justified since the permeabilities and cumulative event count varied over 2 orders of magnitude, respectively. The Locharbriggs sandstone test at 3.0×10^{-5} s^{-1} showed a relatively smaller increase in permeability and AE activity. Initially, permeability and AE event count were negatively correlated. The cumulative event count of 300 events defined a critical state of damage, after which permeability and AE count were positively correlated. Such critical damage is perhaps related to the onset of dilatancy in the test specimen. The Locharbriggs sandstone permeability k and AE events N were related by a log linear relationship given by

$$k = 1.67 \times 10^{-14} \log N + 3.75 \times 10^{-13} \tag{9}$$

where the r^2 value was 0.96. It is possible that the data would also fit equation (8), but a wider bandwidth of N and k would be required to establish this formally.

3.5. Relationship Between Chemical Reaction and Permeability Change

[26] The permeability data for the 80°C slow strain rate tests on Clashach sandstone did not appear to correlate with AE activity or applied load, as shown in Figure 6. Instead, at strain rates of 10^{-7} and 10^{-8} s^{-1} the permeability evolution was more closely related to the chemical state of the system. Figure 6 illustrates this strong correlation of permeability with the concentration of silica in the exit pore water. Initially, compactive processes caused a dramatic 75% reduction in permeability while silica concentration decreased from 20 to 4 ppm. For the 5-day duration of the linear elastic phase, silica concentration remained approximately constant, while permeability values showed a small increase. After the peak stress has been attained, Si concentration peaked while permeability remained at the prepeak level. The formation of a throughgoing fault resulted in a transient increase in permeability due to the suction pump effect of *Grueschow et al.* [2003]. During the frictional sliding phase both silica concentration and permeability decreased rapidly. The sample permeability was directly correlated with Si concentration up to the peak stress of the specimen as well as in the postfailure stage, as shown in Figure 7. The absence of a clear correlation between permeability and dissolved ions at the postpeak

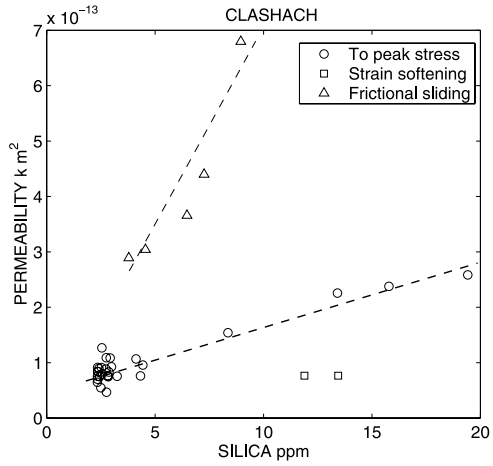

Figure 7. Evolution of permeability and silica concentration for a Clashach sandstone test conducted at a strain rate of 3.3×10^{-8} s^{-1}. Up to peak stress the fluid permeability is a linear function of the concentration of dissolved silica in the exit pore fluid. At strain-softening phase the silica concentration attains a maximum, but the sample permeability remains at a prepeak level. After sample failure the permeability and silica signal are again correlated by a linear law.

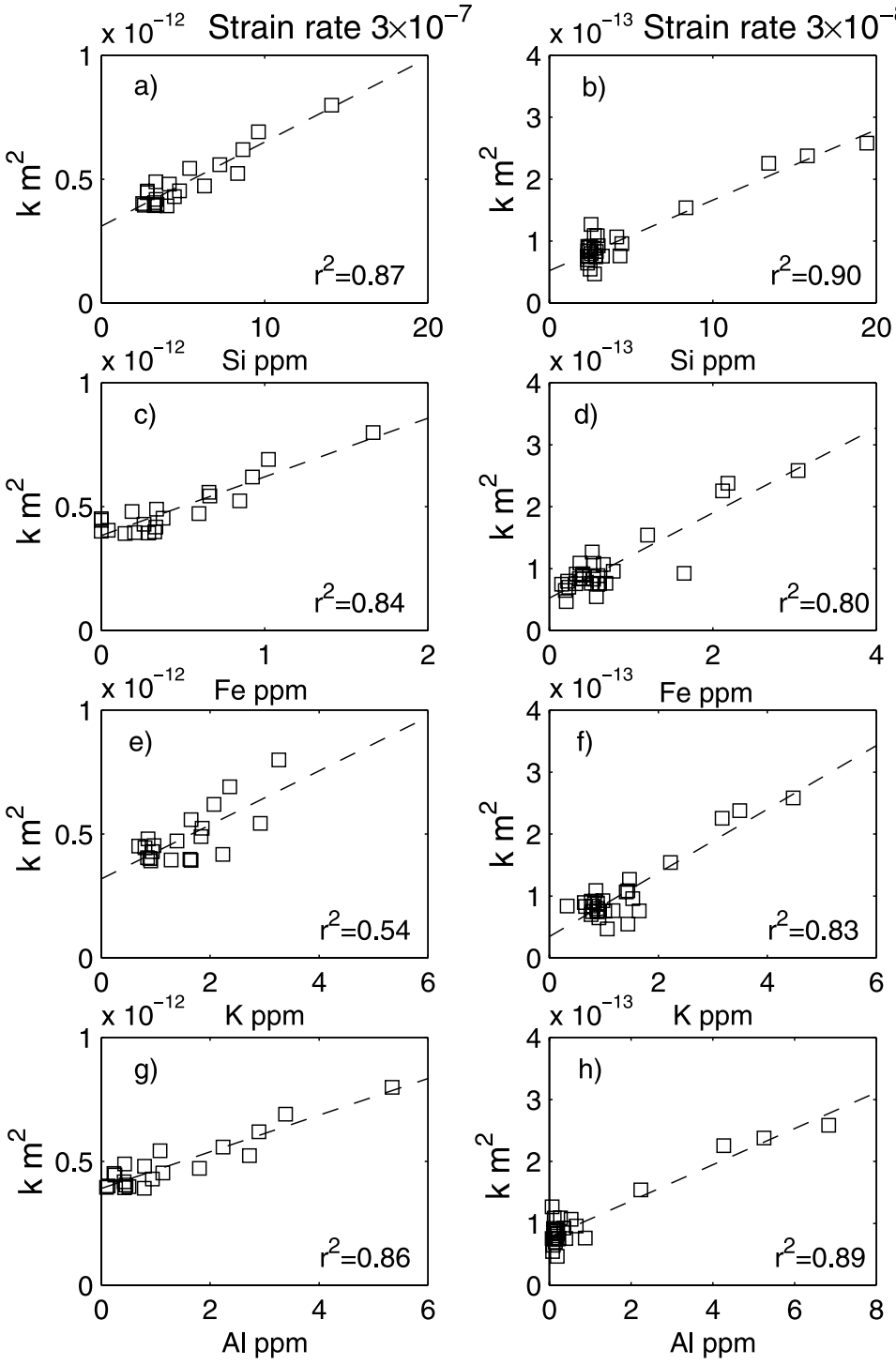

Figure 8. Concentration of dissolved ions as a function of permeability for Clashach sandstone. Axial permeability is a linear function of ion concentration.

region is perhaps related to the onset of shear localization, which may affect these properties differently.

[27] The relation between permeability k and ion concentration C is consistent with a linear law of the form

$$k = \alpha C + \beta \tag{10}$$

where α and β are constants, k is in m^2 and C is in ppm. Such linear dependence of permeability on ion concentrations was observed up to the peak stress σ_{max} and to 95% of σ_{max} for the 10^{-7} and 10^{-8} s^{-1} tests, as shown in Figure 8. For these tests, permeability correlated with the concentrations of Si, Al, K, Fe, and Mg in the exit pore water. Least squares regression was used to obtain the α values that are listed in Table 5. The corresponding correlation coefficients ranged from 0.54 to 0.90. Although the numerical value of α for each ion was different for the two tests, the relative change remained similar, with Si, Al, K, Fe, and Mg

Table 5. Permeability of the Intact Rock Specimen Scales Linearly With Respect to the Exit Ion Concentrations for the Clashach Sandstone Slow Strain Rate 80°C Tests That Were Carried Out at Loading Rate of 10^{-7} and 10^{-8} s^{-1}[a]

Strain Rate, s^{-1}	Element	$\alpha \times 10^{-14}$	r^2
3.3×10^{-7}	Si	3.40	0.874
	Al	7.40	0.863
	K	10.9	0.539
	Fe	23.7	0.840
	Mg	39.3	0.868
3.3×10^{-8}	Si	1.14	0.895
	Al	2.92	0.887
	K	5.14	0.833
	Fe	6.87	0.803
	Mg	8.96	0.535

[a]The axial permeability (in m^2) is given by equation (10) in terms of exit ion concentration (in ppm). The fitted values of were obtained using least squares regression. The r^2 value indicates the goodness of fit of the model.

displaying increasing values of α (in that order). Throughout the tests, Si displayed the highest concentrations while Mg concentrations were the lowest, thus explaining the observed variation in α. The presence of Si, Al, K, Fe, and Mg in the pore water can be attributed to dissolution from quartz, feldspar, illite, and diagenetic iron in the test specimen. The observed positive correlation between sample permeability and fluid ion concentration suggests that the processes of fluid flow and chemical reaction are interrelated at slow strain rates.

[28] In contrast, the Locharbriggs sandstone sample permeability and ion concentration were correlated only at the initial phase of inferred compaction, as illustrated in Figure 9. The closure of favorably oriented microcracks may have resulted in smaller available surface area for dissolution, hence the decreasing concentrations. Both silica (Figure 10) and magnesium concentrations were found to obey a linear law with respect to permeability during the mechanical compaction phase. The fitted coefficients and the associated correlation coefficients for the Locharbriggs tests are shown in Table 6. The variation in Si, Mg, and Fe

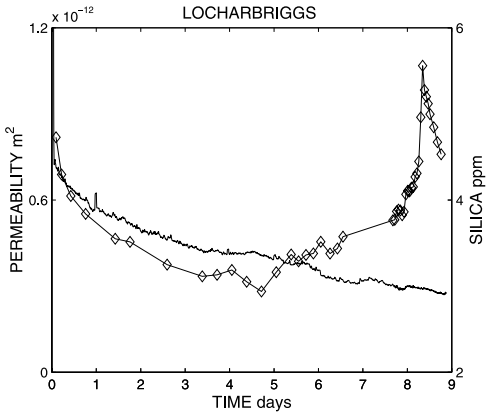

Figure 9. Evolution of silica dissolution (diamond symbols) and permeability for a Locharbriggs sandstone 80°C test carried out at a strain rate of 2.8×10^{-8} s^{-1}. Initially, axial permeability of the test specimen is related to the amount of dissolved silica in the exit pore water.

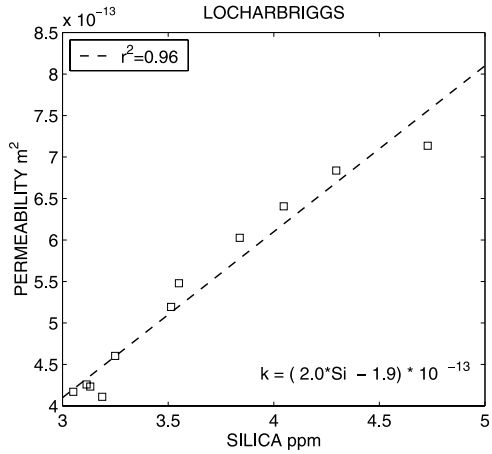

Figure 10. Axial permeability as a function of silica concentration in the exit pore fluid during the initial compaction phase for Locharbriggs sandstone. The test was carried out at a 80°C with a strain rate of 2.8×10^{-8} s^{-1}.

concentrations in the exit pore water can be attributed to dissolution from quartz, illite, and hematite.

4. Discussion

[29] The results of our experiments demonstrate that the permeability evolution of Locharbriggs and Clashach sandstones is affected by the rate at which deformation is occurring. This is an important observation, since most of the previous work has been carried out at room temperature conditions using single deformation rate in the range 10^{-5} to 10^{-6} s^{-1} [*Zhu and Wong*, 1997; *Main et al.*, 2000; *Ngwenya et al.*, 2003]. However, it is well known that the mechanical properties of rocks depend on the deformation rate [*Sano et al.*, 1981; *Costin*, 1987] and much of this time dependence can be attributed to subcritical crack growth [*Atkinson and Meredith*, 1987]. Such time-dependent brittle deformation is the likely cause of the greater linear crack densities and the associated reduction in the elastic modulus in the slow strain rate tests [*Ojala et al.*, 2003]. Subcritical crack growth modifies the pore space and may be responsible for the time-dependent permeability evolution in our tests. Strain rate-dependent permeability evolution has also been previously observed by *Heiland* [2000], who carried out triaxial compression tests on low-porosity (6–9%)

Table 6. Concentration of Silica as a Function of Permeability for Locharbriggs Sandstone During the Initial Compaction Phase[a]

T	$\dot{\varepsilon}$	Ion	$\alpha \times 10^{-13}$	$\beta \times 10^{-13}$	r^2
25	3.3×10^{-7}	Si	3.09	0.16	0.778
40	2.8×10^{-7}	Si	14.2	−7.58	0.843
		Mg	56.9	3.51	0.752
60	3.1×10^{-7}	Si	17.8	−2.38	0.738
80	3.4×10^{-7}	Si	0.27	−1.10	0.923
		Fe	1.58	−0.16	0.540
		Mg	8.10	0.25	0.646
80	2.8×10^{-8}	Si	2.03	−1.90	0.956

[a]Axial permeability is a linear function (equation (10)) of the exit pore fluid concentration. For two tests, the concentrations of magnesium and iron also scale with permeability.

sandstones. In their tests, a deformation rate of 10^{-6} s^{-1} or higher resulted in permeability increase during the dilatant microcracking phase of deformation. In contrast, strain rate of 10^{-7} s^{-1} or less did not lead to a permeability increase, although dilatancy occurred. Our results for Locharbriggs sandstone are in excellent agreement with their observations. In the 10^{-5} to 10^{-6} s^{-1} tests, permeability increases prior specimen failure, while the 10^{-7} and 10^{-8} s^{-1} tests are characterized by continuously decreasing permeabilities. For the Clashach tests, loading rate does not appreciably change the basic pattern of permeability evolution. The relative permeability changes, however, are strongly affected by the deformation rate.

[30] All of the tests are characterized by initial permeability decrease that can be attributed to compaction of pore space and favorably oriented cracks. An initial permeability reduction and an associated decrease in porosity, which continues up to the point C', have also been observed in previous tests on porous sandstones [*Zhu and Wong*, 1997]. While the pore space of a clastic rock is made on three types of pores (nodal pores, tubular pores, cracks), it is the sheet-like microcracks that close most easily due to their greater stress sensitivity [*Bernabé*, 1991; *Zhu and Wong*, 1996]. Although we did not measure volumetric strain, it is assumed that the initial permeability reduction is caused by such compactive processes. The initial decrease in ion concentrations also supports this view since the effect of decreasing porosity is to reduce the available surface area for chemical dissolution.

[31] The initial permeability reduction is more pronounced for the slow strain rate tests than for the high strain rate tests. For both sandstones the ratio of peak stress permeability k_{peak} to initial permeability k_0 decreases with decreasing loading rate (Table 1). In addition, the amount of initial permeability reduction for Clashach sandstone increases systematically with decreasing loading rate (Figure 4). The longer time available for the slow strain rate tests may have resulted in more efficient mechanical compaction in the early stages of loading. Such mechanism was suggested by *Sangha and Dhir* [1972] in order to explain the results of their the creep tests on Laurencekirk sandstone. At a strain rate of 10^{-7} s^{-1} they observed a recovery in lateral strains, which they attributed to a greater degree of compaction attained at a slower strain rate test. Alternatively, a larger initial permeability loss could have been induced by more effective precipitation of low-temperature minerals, such as clay, in the low strain rate tests [*Tenthorey et al.*,1998]. Since our test specimen were impregnated with resin shortly after their removal from the experimental apparatus, we could not test this hypothesis by SEM analysis of fresh surfaces. However, the occurrence of any significant precipitation in our tests is unlikely due to the relatively low temperatures and short durations of the experiments.

[32] Following the initial compaction phase, the sample permeability correlates with AE activity, stress, or chemical content of the exit pore water depending on the strain rate used for the test. In the slow strain rate tests at 80°C, Clashach sandstone exhibits increasing permeabilities prior to faulting, while the permeability of Locharbriggs sandstone decreases continuously. The contrasting permeability evolution of the two sandstones can be explained by their deformation microstructures. The pervasive cracking and grain crushing suggest that brittle fracturing dominates the deformation behavior of the Clashach specimen. Locharbriggs sandstone shows more evidence of grain translation, which may be indicative of a deformation style controlled by compactive processes.

[33] At high strain rates of 10^{-5} to 10^{-6} s^{-1}, permeability is a function of the cumulative AE event count N. Assuming that N is proportional to the inelastic volumetric strain, equations (8) and (9) predict a power law and logarithmic dependence of porosity on permeability for Clashach and Locharbriggs sandstones, respectively. The noninteger exponent in equation (8) suggests that porosity is a fractal object, in accordance with *Thompson* [1991]. Similar power law dependence of permeability on texture is also predicted by the Carman-Kozeny equation [*Carman*, 1956], which is frequently used in estimating permeability in reservoir simulation. Our results imply that during triaxial compression, a positive correlation between porosity and permeability exists under high strain rate loading. However, at crustal strain rate of 10^{-14} to 10^{-16} s^{-1} such relationship may no longer be applicable. Furthermore, the initial permeabilities (Figure 1) do not show any clear correlation with the initial porosities of the test specimen.

[34] At low strain rates of 10^{-7} to 10^{-8} s^{-1} the permeability of Locharbriggs sandstone decreases exponentially with the effective mean stress or axial strain. Similar behavior is observed for the 25–60°C Clashach tests. Such stress- and strain-dependent permeability evolution in sandstone specimens has also been previously reported [*David et al.*, 1994; *Main et al.*, 2000] The stress sensitivity parameter γ_1 varies between 0.45 and 2.93×10^{-2} MPa^{-1}. Some of the γ_1 values observed in our tests are higher than the 0.02 MPa^{-1} limit for porous sandstones suggested by [*Wong and Zhu*, 1999]. However, the 16.1–42.0 obtained for the strain sensitivity coefficient γ_2 lie in the broad region of reported values by [*Ngwenya et al.*, 2003]. The continuously decreasing permeabilities are likely caused by mechanical compaction, such as the clogging of pore throats by fine particles. It has been shown by *Liakopouloux-Morris et al.* [1994] that purely mechanical processes can lead to continuously decreasing permeability in oil-saturated Clashach sandstone.

[35] The 80°C slow strain rate Clashach tests are characterized by permeabilities that do not correlate with stress or AE activity but with the concentrations of dissolved ions in the exit pore fluid. The relationship between sample permeability and ion concentration can be described by a linear law (equation (10)) up to the peak stress σ_{max} and 95% σ_{max} for the 10^{-8} and 10^{-7} s^{-1} tests, respectively. The linear relationship equation (10) is dominated by the large initial reduction in permeabilities and concentrations due to compactive processes. During the linear elastic and strain-hardening phases of deformation the permeability and concentration changes are relatively small when compared to the large reductions associated with the initial compaction and frictional sliding stages (Figure 6). It appears that the microstructural properties of the pore space that control fluid flow are not significantly altered during the linear elastic and strain-hardening phases. Although speculative, the newly formed cracks, as evidenced by the AE activity, may not be efficiently incorporated into the interconnected

porosity traversed by the pore fluid. Such an assumption lends support to the idea that permeability is not only a function of dilatancy but also of microcrack linkage [*Zoback and Byerlee*, 1975; *Zhu and Wong*, 1999; *Popp et al.*, 2001]. Alternatively, only a small proportion of interconnected pore space may dominate the fluid flow [*David et al.*, 1994] and the observed changes in permeability and pore fluid chemistry.

[36] Any thermally induced permeability changes that we observe are small due to the narrow range of temperatures that was used in our tests. Although there is a tendency for the permeability to decrease with increasing temperature (Figure 3a), this effect is not reproduced in all of our tests. However, the permeability evolution of Clashach sandstone displays a clear dependence on the test temperature. While the 25–60°C tests exhibit continuously decreasing permeabilities due to compactive processes, at 80°C the enhanced dissolution rates may have played a dominant role in modifying the pore microstructure and hence fluid flow properties. As a consequence, the 80°C slow strain rate tests display correlation between permeability and the pore water chemistry.

[37] Essentially, the applied loading rate measures the effect of time on the fluid flow and brittle deformation properties during the triaxial compression tests [*Yanagidani et al.*, 1985]. While the very low strain rates operating in the crust are unattainable in laboratory conditions, a slower rate of loading in a conventional test approaches creep strain rates, and it is more representative of the crustal conditions. Our results indicate that a single parameter, such as rock porosity, cannot be used alone to predict the evolution of fluid flow properties during the dilatant microfracturing phase of deformation. Instead, dilatancy can be accompanied by increasing or decreasing permeabilities depending on the applied loading rate. Furthermore, the evolution path for permeability may also change with temperature and notably due to the different diagenetic cements in the otherwise similar rock types examined here. These observations suggest that the evolution of permeability with brittle fracturing can be considerably different in a slow strain rate, high-temperature upper crustal environment than what is typically observed in high strain rate laboratory test carried out at room temperature. In particular, pore fluid chemistry may be directly coupled to the evolution of fluid flow properties in a high-temperature (80°C) slow strain rate environment, as is observed in the Clashach tests.

5. Conclusion

[38] The results of our experiments on Clashach and Locharbriggs sandstones demonstrate that the evolution of permeability depends on the applied loading rate. This is not surprising since the mechanical properties of rocks are characterized by their notable dependence on the deformation rate. Initially, all tests show a decrease in axial permeability, which is likely to be caused predominantly by the closure of favorably oriented compliant microcracks. The amount of initial permeability reduction increases with decreasing loading rate. For Clashach sandstone tests at 80°C the observed permeability reduction displays a linear dependence on the logarithm of strain rate, hence suggesting that a greater degree of initial compaction was attained in the lower strain rate tests.

[39] Following the initial permeability decrease, fluid flow properties evolve as a function of mean effective stress, axial strain, AE damage, or ion concentration depending on the temperature and strain rate used for the test. The high strain rate tests at 10^{-5} and 10^{-6} s^{-1} show a permeability increase, which correlates with the microcrack damage derived from the AE data set. The relationship between AE damage and permeability can be described using a power law and a logarithmic law for the Clashach and Locharbriggs tests, respectively.

[40] The Locharbriggs sandstone slow strain rate tests at 10^{-7} and 10^{-8} s^{-1} exhibit permeabilities that decrease exponentially with the applied axial strain or mean effective stress. Both of these parameters provide equally good fit to the observed data. The stress-dependent permeability evolution suggests that elastic pore closure is responsible for the observed permeability reduction. In contrast, the recorded permeabilities for the slow strain rate 80°C Clashach tests are directly proportional to the concentration of dissolved ions in the exit pore water. Hence chemical reaction may also play a dominant role in modifying the pore microstructure and the fluid flow properties, particularly at slow strain rates. Hence lithology, temperature, and strain rate act together in determining the evolution of fluid flow properties during brittle deformation of porous sandstones. As a consequence, permeability cannot be considered a simple function of porosity when modeling fluid flow properties in high-temperature, slow strain rate crustal conditions.

[41] **Acknowledgments.** We would like to thank Sabrina Colombo, Stephen Elphick, and Nick Odling for their kind assistance in setting up the experimental configuration; Alexander Hart, Robert Brown, Denis McLaughlin, Alex Jackson, and Gavin Brown, who provided valuable technical support; and Nicola Cayzer for help with the SEM. Constructive comments by David Mainprice, Wenlu Zhu, and Till Popp improved the paper substantially. This work was funded by Edinburgh University College of Science and Engineering, The Finnish Cultural Foundation and the Vilho, Yrjö and Kalle Väisälä Foundation.

References

Aharonov, E., E. Tenthorey, and C. H. Scholz (1998), Precipitation sealing and diagenesis: 2. Theoretical analysis, *J. Geophys. Res.*, *103*, 23,969–23,981.

Atkinson, B. K., and P. G. Meredith (1987), The theory of subcritical crack growth with applications to minerals and rocks, in *Fracture Mechanics of Rock*, edited by B. K. Atkinson, pp. 111–166, Academic, San Diego, Calif.

Bernabé, Y. (1991), Pore geometry and pressure dependence of the transport properties in sandstones, *Geophysics*, *56*, 436–446.

Bernabé, Y. (1995), The transport properties of networks of cracks and pores, *J. Geophys. Res.*, *100*, 4231–4241.

Bourbie, T., and B. Zinszner (1985), Hydraulic and acoustic properties as a function of porosity in Fontainebleau sandstone, *J. Geophys. Res.*, *90*, 11,524–11,532.

Brace, W. F. (1980), Permeability of crystalline and argillaceous rocks, *Int. J. Rock Mech. Min. Sci. Geomech. Abstr.*, *17*, 241–251.

Brace, W. F., B. W. Paulding, and C. H. Scholz (1966), Dilatancy in the fracture of crystalline rocks, *J. Geophys. Res.*, *71*, 3939–3953.

Carman, P. C. (1956), *Flow of Gases Through Porous Media*, Butterworths, London.

Clennell, M. B. (1997), Tortuosity: A guide through the maze, in *Developments in Petrophysics*, edited by M. A. Lovell and P. K. Harvey, *Geol. Soc. Spec. Publ.*, *122*, 299–344.

Costin, L. S. (1987), Time-dependent deformation and failure, in *Fracture Mechanics of Rock*, edited by B. K. Atkinson, pp. 167–215, Academic, San Diego, Calif.

Crawford, B. R., B. G. D. Smart, I. G. Main, and F. Liakopoulou-Morris (1995), Strength characteristics and shear acoustic anisotropy of rock core subjected to true triaxial compression, *Int. J. Rock Mech. Min. Sci. Geomech. Abstr.*, *32*, 189–200.

Darcy, H. (1856), *Les Fontaines Publique de la Ville de Dijon*, Dalmont, Paris.

David, C., T.-F. Wong, W. Zhu, and J. Zhang (1994), Laboratory measurements of compaction-induced permeability change in porous rocks: Implications for the generation and maintenance of pore pressure excess in the crust, *Pure Appl. Geophys.*, *143*, 425–456.

Fatt, I. (1956), The network model of porous media, *Trans. Am. Inst. Min. Eng.*, *207*, 144–181.

Grueschow, E., O. Kwon, I. G. Main, and J. W. Rudnicki (2003), Observation and modelling of the suction pump effect during rapid dilatant slip, *Geophys. Res. Lett.*, *30*, 1226, doi:10.1029/2002GL015905.

Guéguen, Y., and J. Dienes (1989), Transport properties of rocks from statistics and percolation, *Math. Geol.*, *21*, 1–13.

Guéguen, Y., and V. Palciauskas (1994), *Introduction to the Physics of Rocks*, Princeton Univ. Press, Princeton, N. J.

Heiland, J. (2000), Permeability in triaxially stressed sandstone, in *Thermo-hydro-mechanical Coupling in Fractured Rock*, edited by K. Hans-Joachim, Basel, Boston, Mass.

Huenges, E. J., J. Erzinger, J. K'uck, B. Engeser, and W. Kessels (1997), The permeable crust: Geohydraulic properties down to 9101 m depth, *J. Geophys. Res.*, *102*, 18,255–18,265.

Kiyama, T., H. Kita, Y. Ishijima, T. Yanagidani, K. Aoki, and T. Sato (1996), Permeability in anisotropic granite under hydrostatic compression and triaxial compression including post-failure region, *Proc. N. Am. Rock Mech. Symp.*, *2*, 1161–1168.

Liakopoulou-Morris, F., I. G. Main, B. R. Crawford, and B. G. D. Smart (1994), Microseismic properties of a homogeneous sandstone during fault nucleation and frictional sliding, *Geophys. J. Int.*, *119*, 219–230.

Lockner, D. A. (1993), The role of acoustic emission in the study of rock fracture, *Int. J. Rock Mech. Min. Sci. Geomech. Abstr.*, *30*, 883–899.

Main, I. G., O. Kwon, B. T. Ngwenya, and S. C. Elphick (2000), Fault sealing during deformation-band growth in porous sandstone, *Geology*, *28*, 1131–1134.

Moore, D. E., C. A. Morrow, and J. D. Byerlee (1983), Chemical reactions accompanying fluid flow in granite held in a temperature gradient, *Geochim. Cosmochim. Acta*, *47*, 445–453.

Mordecai, M., and L. H. Morris (1971), An investigation into the changes of permeability in a sandstone when failed under triaxial conditions, in *Proc. U.S. Rock Mech. Symp.*, *12*, 221–239.

Morrow, C., D. Lockner, D. Moore, and J. Byerlee (1981), Permeability of granite in a temperature gradient, *J. Geophys. Res.*, *86*, 3002–3008.

Morrow, C. A., D. E. Moore, and D. A. Lockner (2001), Permeability reduction in granite under hydrothermal conditions, *J. Geophys. Res.*, *106*, 30,551–30,560.

Ngwenya, B. T., S. C. Elphick, and G. B. Shimmield (1995), Reservoir sensitivity to water flooding: An experimental study of seawater injection in a North Sea reservoir analog, *AAPG Bull.*, *79*, 285–302.

Ngwenya, B. T., O. Kwon, S. C. Elphick, and I. G. Main (2003), Permeability evolution during progressive development of deformation bands in porous sandstones, *J. Geophys. Res.*, *108*, 2343, doi:10.1029/2002JB001854.

Ojala, I., B. T. Ngwenya, I. G. Main, and S. C. Elphick (2003), Correlation of microseismic and chemical properties of brittle deformation properties in Locharbriggs sandstone, *J. Geophys. Res.*, *108*, 2268, doi:10.1029/2002JB002277.

Pape, H., C. Clauser, and J. Iffland (1999), Permeability prediction based on fractal pore-space geometry, *Geophysics*, *64*, 1447–1460.

Paterson, M. S. (1983), The equivalent channel model for permeability and resistivity in fluid-saturated rocks: A re-appraisal, *Mech. Mater.*, *2*, 345–352.

Popp, T., H. Kern, and O. Schulze (2001), Evolution of dilatancy and permeability in rock salt during hydrostatic compaction and triaxial deformation, *J. Geophys. Res.*, *106*, 4061–4078.

Rice, J. D. (1992), Fault stress states, pore pressure distribution and the weakness of the San Andreas fault, in *Fault Mechanics and Transport Properties of Rocks*, edited by B. Evans and T.-F. Wong, pp. 475–504, Academic, San Diego, Calif.

Rudnicki, J. W., and C.-H. Chen (1988), Stabilization of rapid frictional slip on a weakening fault by dilatant hardening, *J. Geophys. Res.*, *93*, 4745–4757.

Sangha, C. M., and R. K. Dhir (1972), Influence of time to the strength, deformation and fracture properties of a lower Devonian sandstone, *Int. J. Rock Mech Min. Sci. Geomech. Abstr.*, *9*, 343–354.

Sano, O., I. Ito, and M. Terada (1981), Influence of strain rate on dilatancy and strength of Oshima granite under uniaxial compression, *J. Geophys. Res.*, *86*, 9299–9311.

Scheidegger, A. E. (1974), *The Physics of Flow Through Porous Media*, Univ. of Toronto Press, Toronto, Ont.

Scholz, C. H. (1968), Microfracturing and the inelastic deformation of rock in compression, *J. Geophys. Res.*, *73*, 1417–1432.

Scholz, C. H., A. Leger, and S. L. Karner (1995), Experimental diagenesis: Exploratory results, *Geophys. Res. Lett.*, *22*, 719–722.

Seeburger, D. A., and A. Nur (1984), A pore space model for rock permeability and bulk modulus, *J. Geophys. Res.*, *89*, 527–536.

Sibson, R. H. (1994), Crustal stress, faulting and fluid flow, in *Geofluids: Origins, Migration and Evolution of Fluids in Sedimentary Basins*, edited by J. Parnell, *Geol. Soc. Spec. Publ.*, *78*, 69–84.

Simpson, G., Y. Gu'eguen, and F. Schneider (2001), Permeability enhancement due to microcrack dilatancy in the damage regime, *J. Geophys. Res.*, *106*, 3999–4016.

Small, J. S., D. L. Hamilton, and S. Habesch (1992), Experimental simulation of clay precipitation within reservoir sandstones 1. Techniques and examples, *J. Sediment. Petrol.*, *62*, pp. 508–519.

Sornette, D. (1999), Earthquakes: From chemical alteration to mechanical rupture, *Phys. Rep.*, *313*, 237–291.

Tapponier, P., and W. F. Brace (1976), Development of stress-induced microracks in Westerley granite, *Int. J. Rock Mech. Min. Sci. Geomech. Abstr.*, *13*, 103–112.

Tenthorey, E., C. H. Scholz, and E. Aharonov (1998), Precipitation sealing and diagenesis: 1. Experimental results, *J. Geophys. Res.*, *103*, 23,951–23,967.

Thompson, A. H. (1991), Fractals in rock physics, *Annu. Rev. Earth Planet. Sci.*, *19*, 137–262.

Walsh, J. B., and W. F. Brace (1984), The effect of pressure on porosity and the transport properties of rock, *J. Geophys. Res.*, *89*, 9425–9431.

Wong, T.-F. and W. Zhu (1999), Brittle faulting and permeability evolution: Hydromechanical measurement, microstructural observation, and network modeling, in *Faults and Subsurface Fluid Flow in the Shallow Crust*, *Geophys. Monogr. Ser.*, vol. 113, edited by W. C. Haneberg, et al., pp. 83–99, AGU, Washington, D. C.

Yanagidani, T., S. Ehara, O. Nishizawa, K. Kusunose, and M. Terada (1985), Localization of dilatancy in Ohshima granite under constant uniaxial stress, *J. Geophys. Res.*, *90*, 6840–6858.

Zhang, S., S. F. Cox, and M. S. Paterson (1994), The influence of room temperature deformation on porosity and permeability in calcite aggregates, *J. Geophys. Res.*, *99*, 15,761–15,775.

Zhu, W., and T.-F. Wong (1996), Permeability evolution in a dilating rock: Network modeling of damage and tortuosity, *Geophys. Res. Lett.*, *23*, 3099–3102.

Zhu, W., and T.-F. Wong (1997), The transition from brittle faulting to cataclasic flow: Permeability evolution, *J. Geophys. Res.*, *102*, 3027–3041.

Zhu, W., and T.-F. Wong (1999), Network modeling of the evolution of permeability and dilatancy in compact rock, *J. Geophys. Res.*, *104*, 2963–2971.

Zhu, W., B. Evans, and Y. Bernabé (1999), Densification and permeability reduction in hot-pressed calcite: A kinetic model, *J. Geophys. Res.*, *104*, 25,501–25,511.

Zoback, M. D., and J. D. Byerlee (1975), The effect of microcrack dilatancy on the permeability of Westerly granite, *J. Geophys. Res.*, *80*, 752–755.

I. G. Main, B. T. Ngwenya, and I. Ojala, School of GeoSciences, University of Edinburgh, Grant Institute, West Mains Road, Edinburgh EH9 3JW, UK. (ira.ojala@glg.ed.ac.uk)